Heliyon 9 (2023) e15286

Contents lists available at ScienceDirect

Heliyon

journal homepage: www.cell.com/heliyon

Research article

Bioinformatic analysis identifies GPR91 as a potential key gene in brain injury after deep hypothermic low flow

Song Puwei [b,1], Xu Jiali [b,1], Deqin Zhuoga [a,1], Wu Kede [b], Nishant Patel [a,b], An Jia [a], Qi Jirong [b,2,**], Mo Xuming [a,b,2,*]

[a] Department of Cardiothoracic Surgery, Nanjing Children's Hospital, Medical School of Nanjing University, Nanjing, 210093, China
[b] Department of Cardiothoracic Surgery, Children's Hospital of Nanjing Medical University, Nanjing, 210008, China

ARTICLE INFO

Keywords:
Brain injury
GPR91
NF-κB
NLRP3
DHCA
Inflammation
Brain ischemia and reperfusion

ABSTRACT

Purpose: Explore the transcription change of brain ischemia and reperfusion injury after deep hypothermic low flow.
Method: The data from PRJNA739516 and GSE104036 were obtained for the differentially expressed genes identification, functional enrichment analysis, gene set enrichment analysis, protein-protein interaction construction and hub gene identification. Oxygen and glucose deprivation model was set to validate the hub gene and explore the detailed brain injury mechanism.
Result: Interleukin, immunological response, NF-κB signaling pathway, G protein-coupled receptor signaling pathway and NLRP inflammatory are functional pathway were enriched in differentially expressed genes analysis. Sucnr1, Casr, Cxcr4, C5ar1, Tas2r41, Tas2r60 and Hcar2 were identified and verified in the OGD model. Knocking down GPR91 reduces the inflammatory response after OGD and GPR91 may be involved in the inflammatory pre-reaction through the synergistic activation of NF-κB, NLRP3, and IL-1β respectively.
Conclusion: Our study found that Interleukin, immunological response, NF-κB signaling pathway, G protein-coupled receptor signaling pathway and NLRP inflammatory are all associated with brain ischemia and reperfusion injury after deep hypothermic low flow and GPR91 can activate NF-κB/NLRP3 pathway and trigger the release of IL-1β in this progress.

Abbreviations: DHCA, Deep Hypothermic Circulatory Arrest; DEGs, Differentially Expressed Genes; CPB, Cardiopulmonary Bypass; MCAO, Middle Cerebral Artery Occlusion; GSEA, Gene Set Enrichment Analysis; GO, Gene Ontology; KEGG, Kyoto Encyclopedia of Genes and Genomes; MCODE, Molecular Complex Detection; OGD, Oxygen and Glucose Deprivation; RNAi, RNA Interference; PBS, Phosphate Buffered Saline; MP, Mononuclear Phagocyte; NSCs, Neural Stem Cells; HCAR1, Hydroxycarboxylic Acid Receptor 1; mRNA, messenger RNA; BCA, Bicinchoninic Acid.

* Corresponding author. Department of Cardiothoracic Surgery, Nanjing Children's Hospital, Medical School of Nanjing University, Nanjing, 210093, China.
** Corresponding author. Department of Cardiothoracic Surgery, Nanjing Children's Hospital, Medical School of Nanjing Children University, Nanjing, 210093, China.
E-mail addresses: qjr7@163.com (Q. Jirong), mohsuming15@njmu.edu.cn (M. Xuming).
[1] Song Puwei, Xu Jiali and Deqin Zhuoga contributed equal efforts and should be listed as co-first authors.
[2] Mo Xuming and Qi Jirong contributed equal efforts and should be listed as co-corresponding authors.

https://doi.org/10.1016/j.heliyon.2023.e15286
Received 16 June 2022; Received in revised form 21 March 2023; Accepted 31 March 2023
Available online 15 April 2023

1. Introduction

Deep hypothermic low flow (DHLF) cardiopulmonary bypass procedure has become more and more prevalent in clinical practice and become routine in complex surgical interventions in recent decades [1]. In the procedure, it decreases core body temperature to 18–22 °C and improves organ resistance to ischemia, which reduces perioperative risk. However, there exhibits hypermetabolism and the brain is intolerant of hypoperfusion and hypoxia which cause the most significant neurological consequences [2–4]. In recent years, numerous studies have been published on the effect of perioperative brain perfusion strategies and temperature control on cerebral protection. However, the underlying mechanisms of neurological disorders are not fully known and require further study [5, 6].

Currently, microarray technology is used to rapidly identify differentially expressed genes (DEGs) related with cerebral ischemia-reperfusion injury which could be also applied to explore the mechanism of brain injury following DHLF. The hub gene is frequently a key target and research hotspot which is defined as a gene that is essential for numerous biological functions [7]. The hub gene frequently affects how other genes in pertinent pathways are regulated [8] and can be screened by calculated with interaction network which is created by the weighted gene co-expression network analysis (WGCNA) or protein-protein interactions (PPI) [9].

Bioinformatics research have demonstrated that numerous hub genes such as CDKN1A, IL-6, FOS, JUN, ATF3, EGR1 help diagnose and treat myocardial injury after DHLF cardiopulmonary bypass (CPB) [10–13]. However, few studies have studied the genes involved in CPB-induced cerebral ischemia and reperfusion injury. This study will examine hub genes to gain a better understanding of cerebral ischemia-reperfusion injury following DHLF-assisted heart surgery. These hub genes may serve as biomarkers or therapeutic targets for DHLF CPB-induced brain injury and will enhance our knowledge of DHLF cerebral ischemia molecular pathways.

2. Method and material

2.1. Microarray dataset collection and DEGs identification

This study examined microarray expression data from the PRJNA739516 bioproject based on the Agilent GPL18694 (https://www.ncbi.nlm.nih.gov/GEO/platform), Illumina HiSeq 2500 (*Rattus norvegicus*), expression profiling supplied five sham and five DHCA procedure groups and GSE104036 based on the Agilent GPL17021 (https://www.ncbi.nlm.nih.gov/GEO/platform), Illumina HiSeq 2500 (*Mus musculus*), expression profiling supplied three sham and nine middle cerebral artery occlusion (MCAO) ipsilateral groups from 6 h to 24 h. The probes were translated into the appropriate gene symbols based on the raw data annotation information. To minimize duplicate testing, each was connected to a separate gene symbol. Although multiple probe sets were related to the same gene, only the probe set with the highest median expression was evaluated [14]. The datasets were normalized as the authors stated [15,16]. Therefore DEGs were identified respectively and $P < 0.05$ and $|\log FC| > 1.5$ were considered as a threshold. The R packages "pheatmap" and "ggplot2," respectively, were used to produce heatmap and volcano plot visualizations.

2.2. DEGs and Gene Set Enrichment Analysis

The result of DEGs enrichment in geneset were obtained from R package 'clusterProfiler (version 3.14.3)' which were applied to perform Gene Ontology (GO) and Kyoto Encyclopedia of Genes and Genomes (KEGG) pathway enrichment analysis. In the meanwhile, the result of Gene Set Enrichment Analysis (GSEA) were calculated by GSEA software (version 3.0) obtained from the GSEA (https://doi.org/10.1073/pnas.0506580102, http://software.broadinstitute.org/gsea/index.jsp) website. We divided the samples into two groups according to the original classification in the dataset, and downloaded the c5.go.bp.v7.4.symbols.gmt subset from the Molecular Signatures Database (DOI: 10.1093/bioinformatics/btr260; http://www.gsea-msigdb.org/gsea/downloads.jsp) to evaluate the relevant pathways and molecular mechanisms. Based on gene expression profile and phenotype grouping, the minimum gene set was set as 5, the maximum gene set was set as 5000, and 1000 times resampling.

2.3. PPI network construction and module analysis

All information on the PPI identified by STRING was analyzed by Metascape, a search engine for detecting interacting genes/proteins. Then, using the Cytoscape program, a PPI network was built and displayed (version 3.7.1). The most important PPI network modules were subsequently determined using Molecular Complex Detection (MCODE) analysis, a Cytoscape APP. MCODE score >3, degree cutoff = 2, node score cutoff = 0.2, and max depth = 100 were the selection criteria.

2.4. Cell culture and transfection

Neuro-2a cells were provided by the Chinese Academy of Sciences' Shanghai Institute of Biotechnology (N2a, mouse neuroblastoma cells) and the mouse N2a cells were cultured in high-glucose Dulbecco's modified Eagle's medium (Gibco, USA) with 10% fetal calf serum (Gibco, USA) at 37 °C in a normoxic 5% CO_2 cell culture incubator. RNA interference (RNAi) is the phenomenon in which tiny molecules of double-stranded RNA selectively degrade homologous messenger RNA (mRNA), thereby blocking or silencing the expression of specific genes. Anhui General Company provided siGPR91 and Lipofectamine RNAiMAX (Invitrogen, USA) was utilized to perform transfection with siGPR91 as directed by the manufacturer. The siRNA sequences: 5′-GCUUCUACUACAAGAUTT-3′ and 5′-AUCUUGUAGUAGAAGCTT-3′ [17].

2.5. Establishment of the oxygen and glucose deprivation (OGD) model

N2a cells were grown for 6 h in glucose-free Dulbecco's modified Eagle's medium (Gibco, USA) at 18 °C in hypoxic conditions before being returned to normal conditions for 24 h. To induce hypoxic conditions, the anaeropack (Mitsubishi Gas Company, Japan) method was applied [18]. N2a cells were grown in glucose-free Dulbecco's modified Eagle's medium before being transferred to an airtight container with an anaeropack, which established a hypoxic environment by absorbing oxygen and releasing CO_2. The medium was then discarded and Dulbecco's modified Eagle's medium with glucose was added, which culture under normoxic conditions for 24 h to induce OGD was resumed. N2a cells were grown in a growth culture medium under normoxic conditions as a control.

2.6. RNA isolation and mRNA quantification

Total RNA was isolated from N2a cells using the TRIzol reagent (Invitrogen, USA) according to the manufacturer's instructions. With NanoDrop ND-2000 equipment (Thermo Fisher, USA), the concentration of the RNA samples was measured using the OD260/OD280 method.

The SYBR-Green Universal Master Mix kit (Vazyme Biotech., China) was used to determine the amounts of mRNAs (Applied Biosystems, USA). GenePharma (Shanghai, China) synthesized primers for Sucnr1, Casr, Hcar2, Cxcr4, C5ar1, IL-1β, IL-17, and TNF-α and the sequences for genes that were synthesized as primers and shown in Table 1. In a 96-well plate, PCRs were incubated for 3 min at 95 °C, then 40 cycles at 95 °C for 15 s and 62 °C for 1 min. The Ct value was used to calculate the relative mRNA expression levels in all samples, which were tested in triplicate. The procedures were conducted in accordance with the Delta-delta Ct analytical method for the relative quantification of the expression of housekeeping genes.

2.7. Cell viability assay

N2a cells (1×10^4 cells/well) were sown in 96-well plates with 100 μL culture media and allowed to attach to the plate's bottom for 24 h. Following the treatments, cell viability was determined using a microplate reader and a cell counting kit-8 (CCK-8, Dojindo, Japan) according to the manufacturer's instructions.

2.8. Western blot and protein quantification

After the indicated treatments, N2a cells were lysed in ice-cold Radio-Immunoprecipitation Assay buffer with a protease inhibitor (Beyotime Biotechnology, China) after Phosphate Buffered Saline (PBS) (Beyotime Biotechnology, China) washing. The Bicinchoninic Acid (BCA) (Beyotime Biotechnology, China) method was used to detect protein concentration at 95 °C modified about 5 min. The proteins in a 30 μg sample were separated by sodium dodecyl sulfate polyacrylamide gel electropheresis (SDS-PAGE), at a voltage of 70 and 120 v, respectively. Equal amounts of proteins were separated using 8% and 15% Sodium Dodecyl Sulfate PolyAcrylamide Gel

Table 1
RNA primer sequences.

β-actin:	
Forward Primer	GGCTGTATTCCCCTCCATCG
Reverse Primer	CCAGTTGGTAACAATGCCATGT
Sucnr1:	
Forward Primer	TCTTGTGAGAATTGGTTGGCAA
Reverse Primer	CATCTCCATAGGTCCCCTTATCA
Casr:	
Forward Primer	CTGACCAGCGAGCCCAAAA
Reverse Primer	GCTGCTACTCCAAAATGGATAGG
Cxcr4:	
Forward Primer	GAAGTGGGGTCTGGAGACTAT
Reverse Primer	TTGCCGACTATGCCAGTCAAG
C5ar1:	
Forward Primer	ATGGACCCCATAGATAACAGCA
Reverse Primer	GAGTAGATGATAAGGGCTGCAAC
Hcar2:	
Forward Primer	CTGGAGGTTCGGAGGCATC
Reverse Primer	TCGCCATTTTTGGTCATCATGT
Tnf-α:	
Forward Primer	CCCTCACACTCAGATCATCTTCT
Reverse Primer	GCTACGACGTGGGCTACAG
IL-1β:	
Forward Primer	GCAACTGTTCCTGAACTCAACT
Reverse Primer	ATCTTTTGGGGTCCGTCAACT
IL-17:	
Forward Primer	TTTAACTCCCTTGGCGCAAAA
Reverse Primer	CTTTCCCTCCGCATTGACAC

Electrophoresis (Beyotime Biotechnology, China) and then transferred to nitrocellulose membranes. Anti-NLRP3, anti-NF-κB, anti-Caspase1, and anti-β-actin (Abcam, USA) primary antibodies were applied to the membranes overnight at 4 °C. To identify the antigen-antibody complexes, the membranes were washed in PBS (0.1% Tween) and treated with horseradish peroxidase-conjugated antigen-antibody complexes using an enhanced chemiluminescence Plus chemiluminescence reagent kit (Beyotime Biotechnology, China).

2.9. Statistical analysis

The information is presented as means with standard deviations (SEs). Student's t-test was used to examine significant differences, as stated in the figure legends. The threshold for statistical significance was set at $p < 0.05$. GraphPad Prism software (Version 8.0.2, San Diego, USA) was used to analyze the data and create relevant visualizations.

3. Results

3.1. Screening of differential genes

After screening of differential genes in PRJNA739516, A total of 914 DEGs between DHCA and sham group were tested, 755 upregulated and 159 downregulated, and DEGs volcano is depicted in Fig. 1A, whereas heatmap plots are depicted in Fig. 1C. In the meanwhile, a total of 517 DEGs between MCAO and sham group were tested in GSE104036, 336 upregulated and 181 downregulated, and DEGs volcano is depicted in Fig. 1B, whereas heatmap plots are depicted in Fig. 1D.

3.2. Functional enrichment analysis of DEGs

Enrichment analysis results of upregulated differential genes of PRJNA739516 DataSet reveal as follows. GO analysis showed that they mainly regulated several biological pathways, including G protein-coupled receptor binding ($p < 0.05$), Interleukin-6 production ($p < 0.01$), Interleukin-1 beta production ($p < 0.01$) and NLRP1 inflammatory ($p < 0.01$) (Fig. 2A) in brain injury. KEGG analysis showed that they mainly regulated two biological pathways, including NF-kappa B signaling pathway ($p > 0.05$) and Primary immunodeficiency ($p < 0.05$) (Fig. 2B) in brain injury.

Enrichment analysis results of downregulated differential genes of PRJNA739516 DataSet reveal as follow. GO analysis showed that they mainly regulated several biological pathways, including Endoplasmic reticulum ($p < 0.01$), Endoplasmic reticulum part ($p < 0.01$) and Mitochondrial envelope ($p < 0.01$) (Fig. 2C) in brain injury. KEGG analysis showed that they mainly regulated several

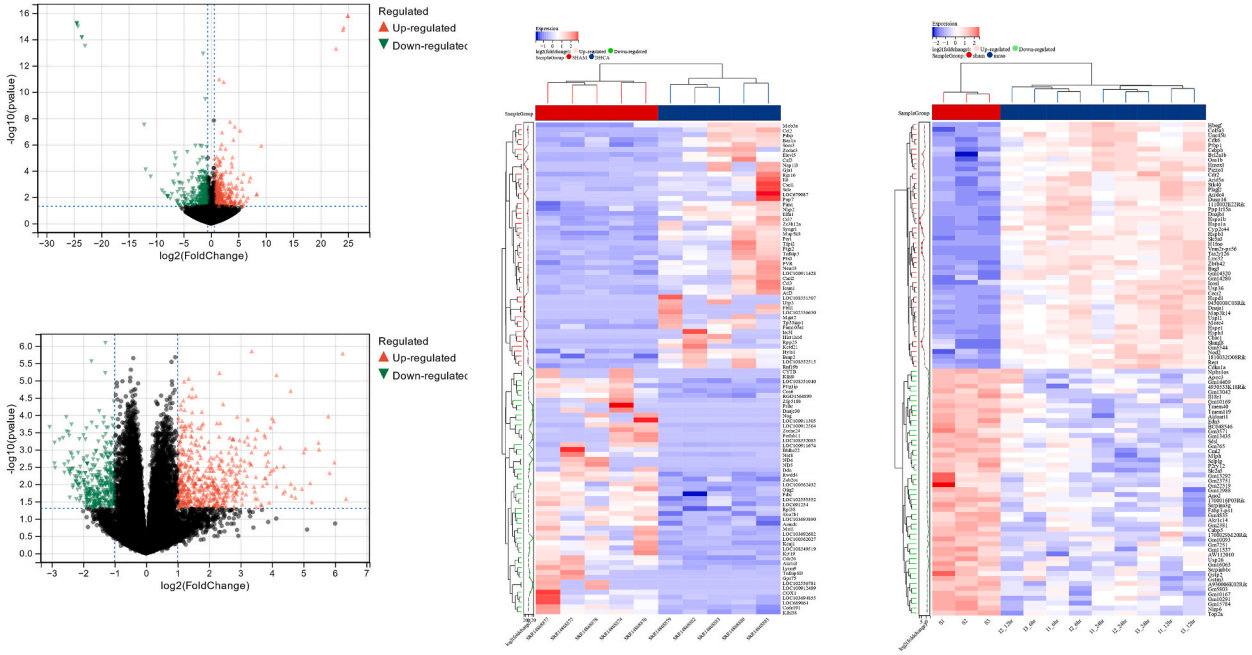

Fig. 1. Screening of Differential Genes. A~B. Volcano map of DEGs in upregulated and downregulated mRNAs of DHCA rat model(A) and mouse brain ischemia/reperfusion model(B). Red represents the selected upregulated genes and green represents the selected downregulated genes. C ~ D. heatmap of DEGs in upregulated and downregulated mRNAs of DHCA rat model(C) and mouse brain ischemia/reperfusion model(D). Red represents the selected upregulated genes and blue represents the selected downregulated genes.

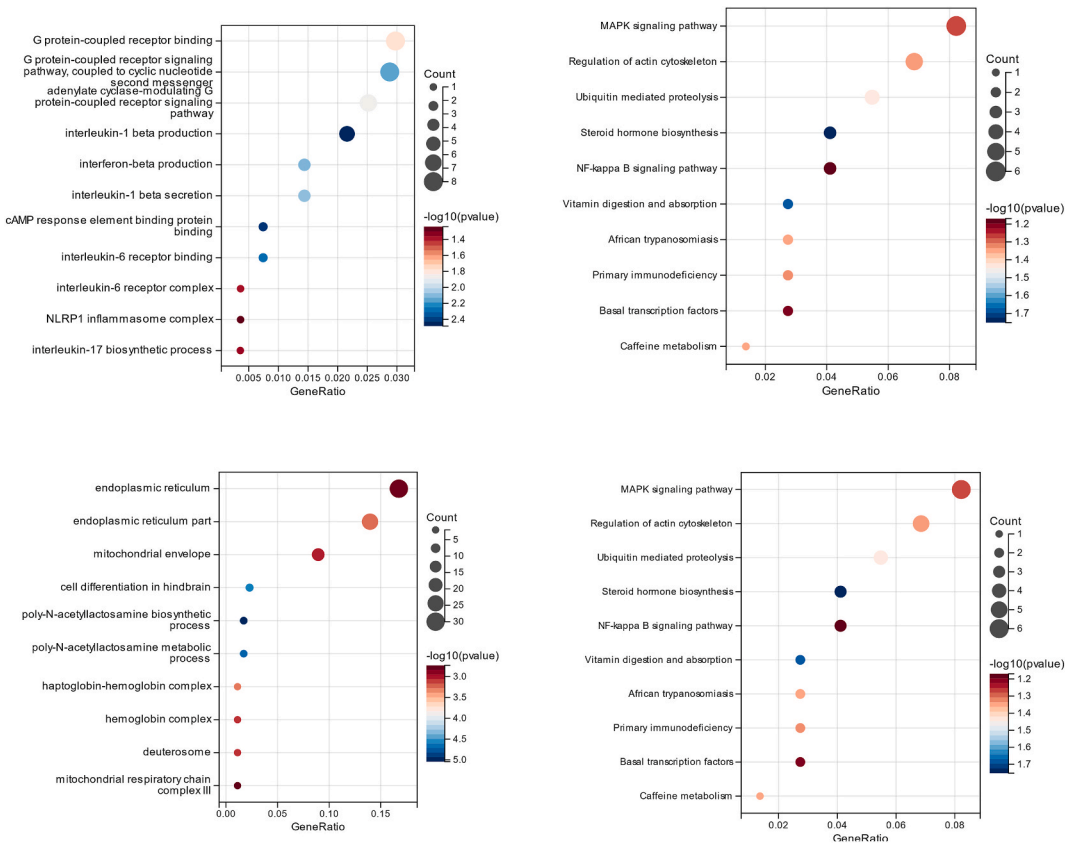

Fig. 2. GO and KEGG Enrichment Analysis of DEGs in DHCA rat model. A~D. Gene Ontology Enrichment of upregulated genes (A), KEGG Enrichment of upregulated genes (B) and Gene Ontology Enrichment of downregulated genes (C), KEGG Enrichment of downregulated genes (D) in DHCA rat model.

biological pathways, including Cytokine-cytokine receptor interaction ($p < 0.01$), TNF signaling pathway ($p < 0.01$) and NF-kappa B signaling pathway ($p < 0.05$) in brain injury (Fig. 2D).

Enrichment analysis results of upregulated differential genes of GSE104036 DataSet reveal as follow. GO analysis showed that they mainly regulated several biological pathways, including Immune response ($p < 0.01$), I-kappaB kinase/NF-kappaB signaling ($p < 0.01$), G protein-coupled receptor signaling pathway ($p < 0.01$) and NLRP3 inflammasome complex ($p > 0.05$) (Fig. 3A) in brain injury. KEGG analysis showed that they mainly regulated several biological pathways, including TNF signaling pathway ($p < 0.01$), NF-kappa B signaling pathway ($p < 0.01$) and Toll-like receptor signaling pathway ($p < 0.01$) (Fig. 3B) in brain injury.

Enrichment analysis results of downregulated differential genes of GSE104036 DataSet reveal as follow. GO analysis showed that they mainly regulated several biological pathways, including Immune response ($p < 0.01$), Receptor ligand activity ($p < 0.01$) and Receptor regulator activity ($p < 0.01$) (Fig. 3C) in brain injury. KEGG analysis showed that they mainly regulated several biological pathways, including Cytokine-cytokine receptor interaction ($p < 0.01$), Viral protein interaction with cytokine and cytokine receptor ($p < 0.01$) and PPAR signaling pathway ($p < 0.01$) (Fig. 3D) in brain injury.

3.3. GSEA enrichment analysis of DEGs

GSEA GO enrichment analysis showed that G protein coupled receptor signaling pathway expression significantly elevated in DHCA (P-value = 0.157) (Fig. 4A) and MCAO (P-value = 0.0753) (Fig. 4C). G PROTEIN COUPLED RECEPTOR BINGDING expression significantly elevated in DHCA (P-value = 0.0258) (Fig. 4B) and MCAO (P-value = 0.0333) (Fig. 4D).

KEGG enrichment analysis of GSEA showed that NF-KB_C (P-value = 0.0435) and NF-KB_Q6_01 expression significantly elevated in DHCA (NF-KB_C P-value = 0.0435; NF-KB_Q6_01 P-value = 0.0453) (Fig. 5A) and MCAO (P-value = 0.0000) (Fig. 5B).

3.4. PPI network construction and module analysis

Metascape was used to establish PPI network in STRING (V11.0) with 499 edges and 247 nodes to investigate the association between protein interactions by those DEGs. According to the STRING analysis, 336 genes were filtered into the DEG PPI network complex (Fig. 6A). The network was visualized using Metascape. Furthermore, the names of the seven hub genes in the top module

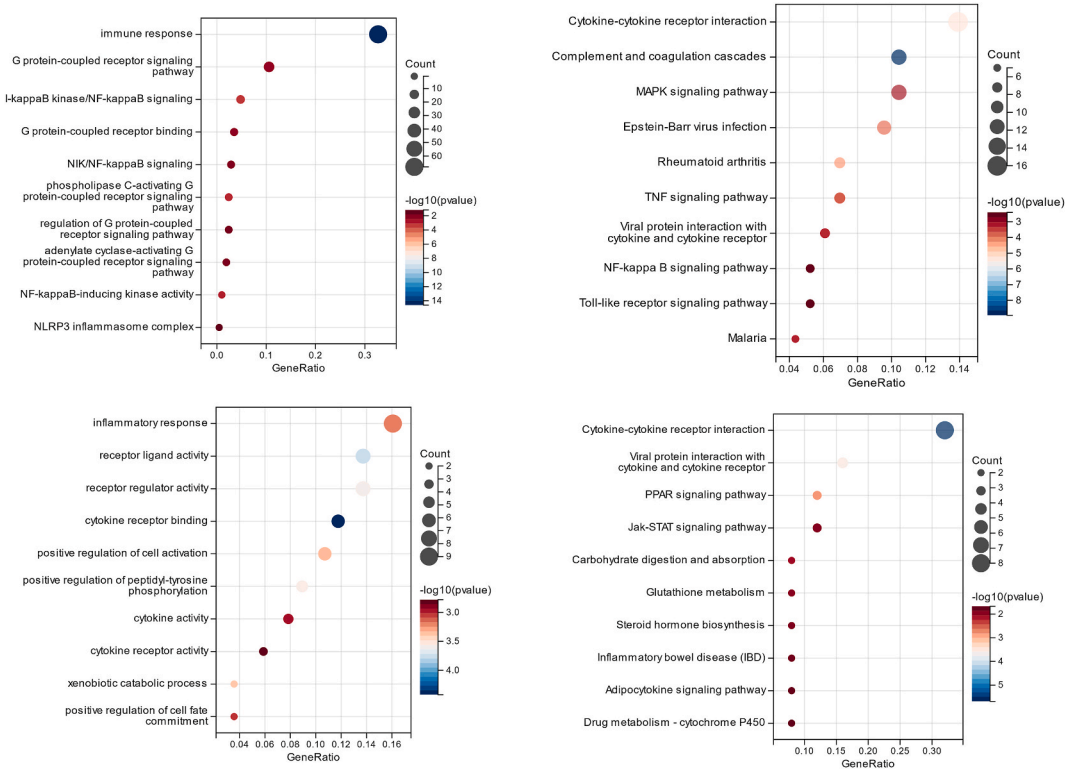

Fig. 3. GO and KEGG Enrichment Analysis of DEGs in mouse brain ischemia/reperfusion model. A∼D. (A) Gene Ontology Enrichment of upregulated genes, (B) KEGG Enrichment of upregulated genes and (C) Gene Ontology Enrichment of downregulated genes, (D) KEGG Enrichment of downregulated genes in DHCA rat model.

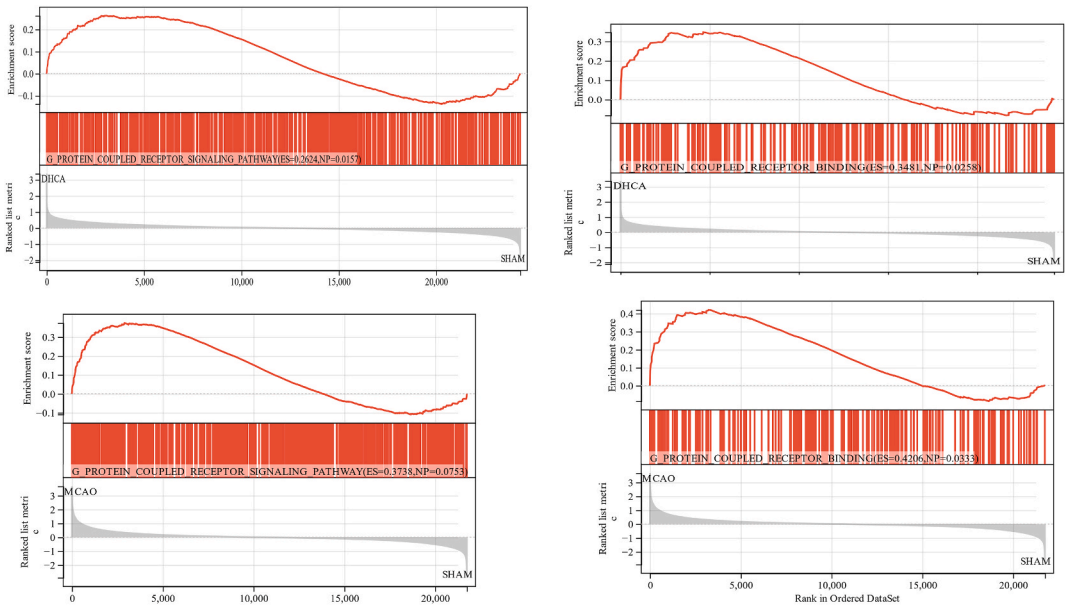

Fig. 4. GO_GSEA Enrichment Analysis of DEGs. A∼B. Biological process(A) and Molecular functions(B) enrichment analysis of DEGs in DHCA rat model. C ∼ D. Biological process(C) and Molecular functions(D) enrichment analysis of DEGs in DHCA rat model.

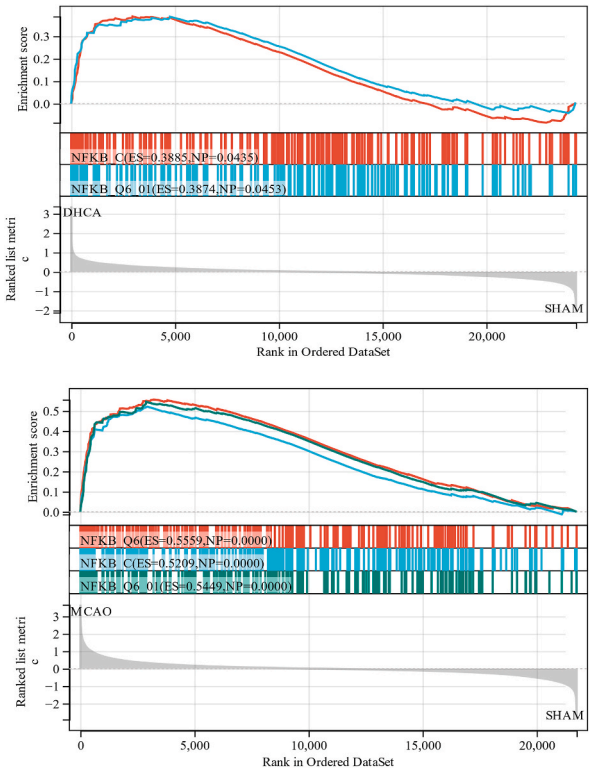

Fig. 5. KEGG_GSEA Enrichment Analysis of DEGs. NF-κB related KEGG Enrichment Analysis of DEGs in DHCA rat model(A) and mouse brain ischemia/reperfusion model(B).

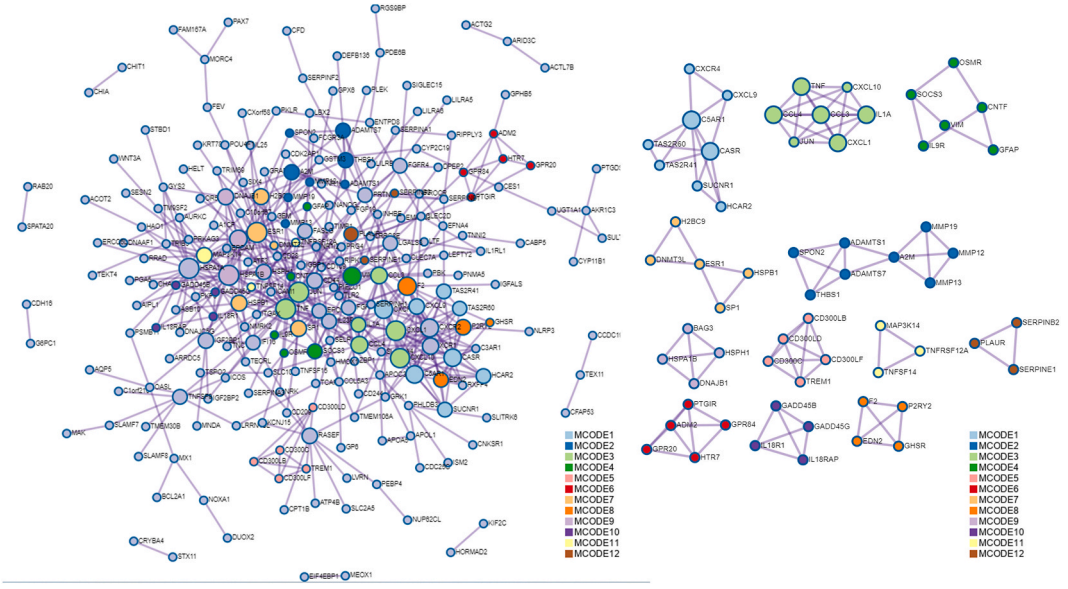

Fig. 6. PPI Network of DEGs Constructed by the STRING Database. A. The PPI network of DEGs was constructed by Cytoscape. B. Identification of sub-network with MCODE in Cytoscape software.

were Sucnr1, Casr, Cxcr4, C5ar1, Tas2r41, Tas2r60 and Hcar2 according to MCODE's module analysis in Cytoscape (Fig. 6B).

3.5. Establishment of OGD model and validation of hub gene expression

OGD was initially established, and different hypoxic and glucose-deprived times (0–8 h) were chosen as the time points. CCK8 cell activity was measured 24 h following reperfusion. At 2 h, the activity of hypoxic glucose-deficient cells increased but dropped dramatically at 6 h. As a result, the 6 h hypoxia glucose deficiency regimen was selected in subsequent tests. (Fig. 7A).

RT–PCR was used to measure the difference in the mRNA level expression of the hub genes before and after modeling. Sucnr1 ($P < 0.001$), Casr ($P < 0.001$), Cxcr4 ($P < 0.001$), C5ar1 ($P < 0.05$), Cxcl9 ($P < 0.05$) and Hcar2 ($P < 0.05$) levels were higher in the OGD group (Fig. 7B–H).

3.6. Knockdown of GPR91 suppresses OGD induced inflammatory factors in N2a cells

We examined the efficacy of small interfering RNA following siGPR91 transfection, and GPR91 expression ($P < 0.01$) was reduced after interference (Fig. 8A). The CCK8 test was used to study the effect of GPR91 on neuronal cell death in vitro. The results ($p < 0.001$) showed that OGD treatment increased neuronal apoptosis, while siGPR91 treatment improved neuronal survival ($p < 0.01$) (Fig. 8B). The levels of proinflammatory cytokines, such as TNF-α, IL-1β, and IL-17 were analyzed using RT–PCR to evaluate whether GPR91 deletion can downregulate specific inflammatory cytokines. The findings showed that compared to the control group, GPR91 deletion reduced the levels of TNF-α($p < 0.01$), IL-1β($p < 0.001$), and IL-17 ($p < 0.001$) (Fig. 8C–E).

In our study, we discovered knockdown of GPR91 lowered the expression level of Nuclear factor-κB (NF-κB), ($p < 0.001$), NLRP3 ($p < 0.001$), and caspase-1 ($p < 0.001$) when compared to the only OGD group ($p < 0.05$) (Fig. 8F–I).

4. Discussion

In clinical, more than half of patients who experience heart surgery with DHLF were observed to have neurological implications [19] and the rat model showed similar result [20,21]. The modulation of transcriptional levels of cerebral ischemia is still uncertain after heart surgery with deep hypothermic technique is still uncertain [22]. Our results revealed that GPR91 plays a significant role in brain ischmia and reperfusion injury after heart surgery with DHLF and inflammation is highly associated.

Firstly, to better understand the transcription change of DHLF, the dataset associated with DHCA and MCAO models were selected. In the enrichment analysis of differential genes, we discovered that DHCA and MCAO up-regulated differential genes GO-enriched the release of interleukin, immunological response, NF-κB signaling pathway, G protein-coupled receptor signaling pathway, and NLRP inflammatory complex. KEGG enrichment analysis of DHCA and MCAO up-regulated differential genes revealed that they were primarily associated with the NF-κB and MAPK signaling pathways. Down-regulated differential genes were also associated with inflammation, cytokines, the PPAR signaling pathway, and the JAK-STAT signaling pathway, according to GO and KEGG enrichment analysis.

Previous studies discovered that cerebral hypoperfusion resulting from reduced cerebral blood flow during CPB produces pro-inflammatory responses, such as the generation of IL-1β from the ischemic endothelium, which leads to increased infarction volumes and exacerbates brain injury. Wang L et al. also believed that inflammatory cytokines are involved with the secondary brain injury in cerebral ischemia and reperfusion, including IL-1β and IL-18 [23].

Besides Qin C. et al. noted that NLRP1 is associated with cerebral ischemic damage and that inhibiting it reduces neuroinflammation in ischemia [24].

In addition, many studies have confirmed that G protein-coupled receptors are involved in the regulation of cerebral ischemia-reperfusion injury. Certain contractile G protein-coupled receptors have been reported to be elevated in brain tissue during ischemia and reperfusion in human cerebral vessels [25]. And it was recently discovered that lactate-activated hydroxycarboxylic acid receptor 1 (HCAR1) (also called the G-protein-coupled lactate receptor GPR81) is present in neurons, glial cells, and cerebral blood arteries throughout the brain [26,27].

Therefore, we believe that the G protein-coupled receptor and the NF-κB signaling pathway play significant roles in DHLF assisted cardiac surgery, and the findings of the GSEA enrichment analysis support our hypothesis.

The brain injury pathogenesis after DHLF is primarily driven by oxidative stress generated by systemic inflammation [28]. Neuroinflammation after heart surgery is known to be influenced by systemic inflammation, which is defined by an increase in inflammatory cytokines which indicated that inflammation may play a major role in our study. Previous reports demonstrated that in individuals treated with DHCA procedure, circulating inflammatory cytokines were increased [29] and in rat DHCA models, serum TNF- α and IL-6 levels were elevated [30]. Moreover, the proinflammatory cytokines IL-6, IL-1β, and TNF-α were increased in plasma and brain regions after DHCA procedure [31–34]. Our enrichment results also discovered multiple signaling pathways such as TNF, IL-17, and cytokine-mediated. Cytokine receptor interaction and proinflammatory and profibrotic mediators were discovered in the biological pathway in the meanwhile.

Afterward, to explore the DEGs interaction relationships, we constructed a PPI network and selected the modules with the highest MCODE scores. Succinate receptor 1 (SUCNR1) and calcium-sensing receptor (CaSR) are two important G protein-coupled receptors [35].CaSR is a G protein-coupled receptor found in the brain that is activated by increased calcium and has a significant impact on serum calcium management. CaSR is expressed by neurons and glial subsets throughout the brain and is activated by extracellular calcium [36]. CaSR is also an important neuronal signaling target [37]. According to Jones and Smith's findings, CaSR modulates

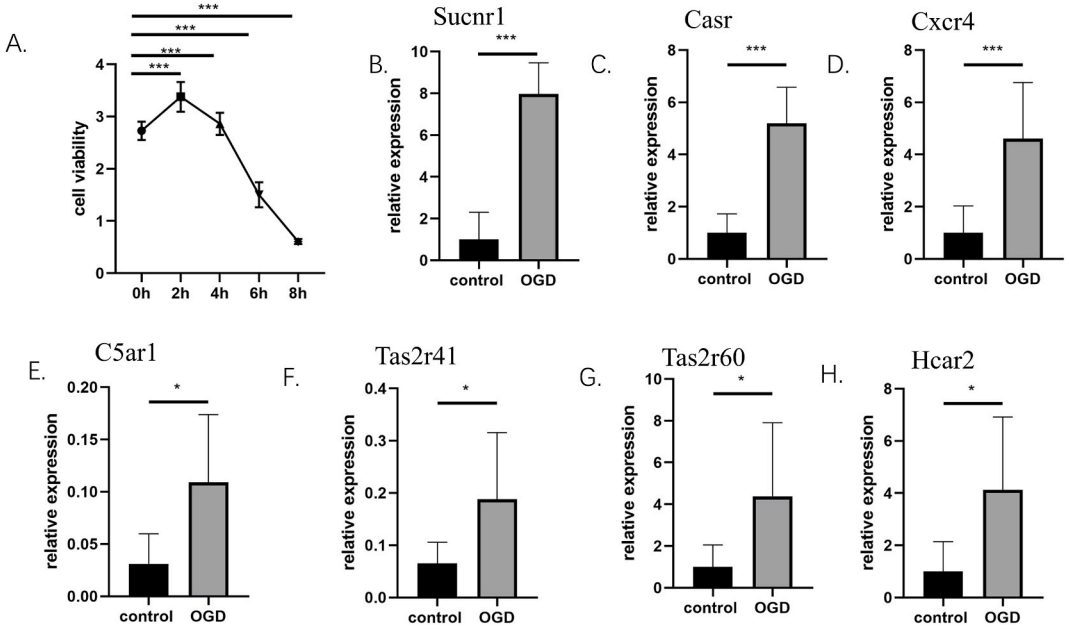

Fig. 7. Establishment of OGD and Experiment Validation of Hub Genes. A. Cell activity detection under different hypoxia times and the 6 h was the selected time point of hypoxia time. B-G. Relative mRNA expression levels of hub genes expression and β-actin was the internal reference. *p < 0.05; **p < 0.01, ***p < 0.001.

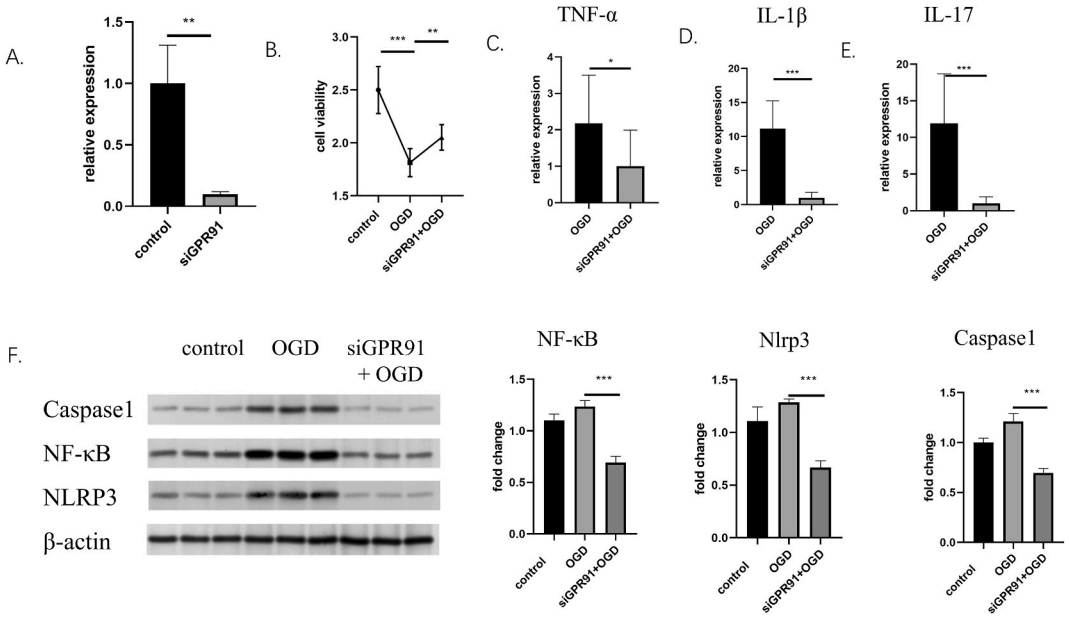

Fig. 8. Knockdown of GPR91 gene and detection of inflammatory indicators. A. GPR91 expression after transfection with siGPR91. B. Cell activity after OGD and siGPR91 OGD model. C-E. Relative mRNA expression level of inflammatory indicators include: TNF-α, IL-1β, IL-17 and β-actin and β-actin was the internal reference. *p < 0.05; **p < 0.01, ***p < 0.001. Inflammatory indicators decreased after siGPR91 transfection. F. Western blot detection of protein NF-κB, NLRP3 and Caspase1 and β-actin and β-actin was the internal reference. G-H. Fold change of the above protein *p < 0.05; **p < 0.01, ***p < 0.001. NF-κB, NLRP3 and Caspase1 decreased after siGPR91 transfection.

intrinsic excitability, synaptic transmission, and neuronal activity, and CaSR is involved in the pathophysiology of acute nervous system illnesses such as stroke, traumatic brain injury, and epilepsy.

SUCNR1, also named GPR91, another hub gene in the top module, is a G-protein-coupled receptor that has been found to regulate cell proliferation, migration, capillary formation, neovascularization, VEGF production, and stem cell activity. SUCNR1 is found in the

kidney, liver, brain, bone marrow, and numerous malignancies [38].

GPR91 and succinate were found to be important contributors to the recovery of newborn brain hypoxia and ischemia in a recent study. By lowering the quantity of succinate in CSF fluid, Luca Peruzzotti-Jametti et al. revealed that transplanted somatic cells and directly produced neural stem cells (NSCs) reduced mononuclear phagocyte (MP) infiltration and secondary CNS injury [39]. Succinate is released by inflammatory MPs, which activate GPR91 on NSCs, resulting in anti-inflammatory actions. Thus, our findings show that the succinate-GPR91 axis plays an unanticipated role in somatic and directly generated NSCs that regulate stem cell responses to inflammatory metabolic signals secreted by type 1 MP in the chronically inflamed brain [40]. By signaling GPR91, extracellular succinate modulates dendritic cell motility to drain lymph nodes and antigen presentation capacity [41]. GPR91 also induces anti-inflammatory responses in macrophages and other cell types [42].

GPR91 expression was found to be linked with the expression of leukocyte markers CD86 and CD206, supporting the connection between inflammation and the succinate- GPR91 pathway [43]. We discovered that GPR91 deletion lowered the inflammatory response following OGD in our study.

GPR91 expression is associated with a multitude of immune-related activities and pathways, including cytokine binding to MHC proteins, cytokine production regulation, immune response process regulation, and interferon/signaling regulation [44].GPR91 reliance on IL-1β expression was found to be higher in synovial fluid from rheumatoid arthritis patients with high succinate levels, indicating that inhibiting GPR91 could be a promising anti-inflammatory target [45]. The association between GPR91 expression and interleukins, including IL-1β, IL-7, IL-16, and IL-18, has been found to be significant [44]. We validated that knocking down GPR91 decreased inflammatory factors in our study.

NF-κB is a significant cause of inflammation [35]. The classical NLRP3 inflammasome pathway consists of two parts. The first part is the activation of TLR4 and myD88, which activates NF-κB and initiated inflammasome gene transcription [46]. The second part is the inflammasome activation of NLRP3/caspase-1/pro-IL-1β and IL-1β. GPR91 may increase the release of high amounts of TNF-α, enhancing inflammation [47]. Early research also showed that GPR91 can boost the inflammatory response in bone marrow cells by acting synergistically with innate Toll-like receptors [48]. However, a previous study demonstrated that GPR91 triggers the NLRP3/caspase-1 cascade, with no effect on NF-κB [49]. In contrast, a previous study also shows that by stimulating GPR91 and NF-κB signal transduction, succinate increased OC osteoclast development and bone resorption [50]. In our study, we have validated that knockdown of GPR91 decreases the protein expression of NF-κB, NLRP3, Caspase-1, and the gene expression of IL-1β.

Therefore, we suggested that GPR91 can activate NF-κB/NLRP3/caspase-1/IL-1β signaling pathway which might trigger inflammation in brain injury after DHCA procedure. More experiments especially in population samples and animal studies are required in the future.

This article was the first to investigate the hub genes involved in DHLF-induced cerebral ischemia-reperfusion injury, laying the groundwork for the mechanism and medication development of brain protection in DHLF-assisted cardiac surgery. Our strength is that we chose N2a cells, developed an OGD model, validated the hub gene, and confirmed the role and mechanism of GPR91 in cerebral ischemia-reperfusion by knocking down the GPR91 gene and detecting inflammation-related proteins. As to the limitations, sequencing of clinical samples from children undergoing DHLF-assisted cardiac surgery was lacking. Only the DHCA and MCAO models, which are similar with the deep hypothermic low flow models, are discussed in this paper, and more direct DHLF models must be built for verification. Furthermore, validation sets are needed to eliminate the effect of gene specificity. In vitro investigations are required to validate the mechanism of the hub gene and the GPR91 gene, and in vivo and in vitro experiments are required to explore more brain-protective mechanisms.

5. Conclusions

Our study found that Interleukin, immunological response, NF-KB signaling pathway, G protein-coupled receptor signaling pathway and NLRP inflammatory are all associated with brain ischemia and reperfusion injury after DHLF procedure and GPR91 can activate NF-κB/NLRP3 pathway and trigger the release of IL-1β in this progress.

Contribution statement

Song Puwei, Xu Jiali and DeQin ZhuoGa conceived and designed the experiments and wrote the paper; Wu Kede performed the experiments; Yang zhaocong, Nishant Patel and An Jia analyzed and interpreted the data and wrote the paper; Mo Xuming and Qi Jirong contributed reagents, materials, analysis tools or data and wrote the paper.

Funding

This work was supported by Postgraduate Research & Practice Innovation Program of Jiangsu Province (KYCX21_1564), the Subproject of the National Key R&D Program "The recognition and identification of genetic pathogenic genes for structural birth defects" (2021YFC2701002), the National Natural Science Foundation of China (81970265, 82000303) and Nanjing Science and Technology Development Project (2019060007).

Declaration of competing interest

The authors declare no conflicts of interest.

Data available statement

The data that support the findings of this study are available from the corresponding author, upon reasonable request.

Acknowledgment

Many thanks to friends accompanied in our postgraduate life.

Appendix A. Supplementary data

Supplementary data to this article can be found online at https://doi.org/10.1016/j.heliyon.2023.e15286.

References

[1] M.A. Ergin, J. O'connor, R. Guinto, et al., Experience with profound hypothermia and circulatory arrest in the treatment of aneurysms of the aortic arch. Aortic arch replacement for acute arch dissections[J], J. Thorac. Cardiovasc. Surg. 84 (5) (1982) 649–655.
[2] M. Cefarelli, G. Murana, G.G. Surace, et al., Elective aortic arch repair: factors influencing neurologic outcome in 791 patients[J], Ann. Thorac. Surg. 104 (6) (2017) 2016–2023.
[3] R. Legre, R. Courbier, M. Zanaret, et al., [Surgical excision of giant venous angioma of the face under extracorporeal circulation: apropos of a case by a multidisciplinary team][J], Ann. Chir. Plast. Esthet. 36 (4) (1991) 297–301.
[4] K. Bartels, Q. Ma, T.N. Venkatraman, et al., Effects of deep hypothermic circulatory arrest on the blood brain barrier in a cardiopulmonary bypass model–a pilot study[J], Heart Lung Circ. 23 (10) (2014) 981–984.
[5] E. Apostolakis, J.H. Shuhaiber, Antegrade or retrograde cerebral perfusion as an adjunct during hypothermic circulatory arrest for aortic arch surgery[J], Expert Rev. Cardiovasc Ther. 5 (6) (2007) 1147–1161.
[6] S. Fan, H. Li, D. Wang, et al., Effects of four major brain protection strategies during proximal aortic surgery: a systematic review and network meta-analysis[J], Int. J. Surg. 63 (2019) 8–15.
[7] M. Shan, H. Liu, K. Song, et al., Immune-related gene expression in skin, inflamed and keloid tissue from patients with keloids[J], Oncol. Lett. 23 (2) (2022) 72.
[8] H. Zhang, C. Bian, S. Tu, et al., Construction of the circRNA-miRNA-mRNA regulatory network of an abdominal aortic aneurysm to explore its potential pathogenesis[J, Dis. Markers 2021 (2021), 9916881.
[9] T. Xu, H. Ruan, Z. Song, et al., Identification of CXCL13 as a potential biomarker in clear cell renal cell carcinoma via comprehensive bioinformatics analysis[J], Biomed. Pharmacother. 118 (2019), 109264.
[10] H. Chen, J. Liu, Y. Wu, et al., Weighted gene co-expression identification of CDKN1A as a hub inflammation gene following cardiopulmonary bypass in children with congenital heart disease[J], Front. Surg. 9 (2022), 963850.
[11] H. Liu, B. Zhang, S. Chen, et al., Identification of ferroptosis-associated genes exhibiting altered expression in response to cardiopulmonary bypass during corrective surgery for pediatric tetralogy of fallot[J], Sci. Prog. 104 (4) (2021), 368504211050275.
[12] H. Liu, Y. Zhang, Z. Wu, et al., Identification of IL-6 as a potential mediator of the myocardial fibrosis that occurs in response to surgery with cardiopulmonary bypass in children with Tetralogy of Fallot[J], Cardiol. Young 32 (2) (2022) 223–229.
[13] Q. Qi, Y. Yan, C. Luo, et al., Bioinformatics analysis reveals hub genes that may reduce inflammation and complications after cardiopulmonary bypass[J], Heart Surg. Forum 25 (2) (2022) E243–E252.
[14] G. Zhou, O. Soufan, J. Ewald, et al., NetworkAnalyst 3.0: a visual analytics platform for comprehensive gene expression profiling and meta-analysis[J], Nucleic Acids Res. 47 (W1) (2019) W234–W241.
[15] M. Kobayashi, C. Benakis, C. Anderson, et al., AGO CLIP reveals an activated network for acute regulation of brain glutamate homeostasis in ischemic stroke[J], Cell Rep. 28 (4) (2019) 979–991 e6.
[16] M. Liang, Y. Zhang, S. Gan, et al., Identifying lncRNA- and transcription factor-associated regulatory networks in the cortex of rats with deep hypothermic circulatory arrest[J], Front. Genet. 12 (2021), 746757.
[17] G. Xu, Y. Yuan, P. Luo, et al., Acute succinate administration increases oxidative phosphorylation and skeletal muscle explosive strength via SUCNR1[J], Front. Vet. Sci. 8 (2021), 808863.
[18] R. Harari-Steinfeld, M. Gefen, A. Simerzin, et al., The lncRNA H19-derived MicroRNA-675 promotes liver necroptosis by targeting FADD[J], Cancers 13 (3) (2021).
[19] A. Levati, C. Tommasino, M.P. Moretti, et al., Giant intracranial aneurysms treated with deep hypothermia and circulatory arrest[J], J. Neurosurg. Anesthesiol. 19 (1) (2007) 25–30.
[20] W. Yang, Q. Ma, G.B. Mackensen, et al., Deep hypothermia markedly activates the small ubiquitin-like modifier conjugation pathway; implications for the fate of cells exposed to transient deep hypothermic cardiopulmonary bypass[J], J. Cerebr. Blood Flow Metabol. 29 (5) (2009) 886–890.
[21] L.T. Loftus, R. Gala, T. Yang, et al., Sumo-2/3-ylation following in vitro modeled ischemia is reduced in delayed ischemic tolerance[J], Brain Res. 1272 (2009) 71–80.
[22] X. Wang, Z. You, G. Zhao, et al., MicroRNA-194-5p levels decrease during deep hypothermic circulatory arrest[J], Sci. Rep. 8 (1) (2018), 14044.
[23] L. Wang, W. Ren, Q. Wu, et al., NLRP3 inflammasome activation: a therapeutic target for cerebral ischemia-reperfusion injury[J], Front. Mol. Neurosci. 15 (2022), 847440.
[24] C. Qin, S. Yang, Y.H. Chu, et al., Signaling pathways involved in ischemic stroke: molecular mechanisms and therapeutic interventions[J], Signal Transduct. Targeted Ther. 7 (1) (2022) 215.
[25] L.I. Edvinsson, G.K. Povlsen, Vascular plasticity in cerebrovascular disorders[J], J. Cerebr. Blood Flow Metabol. 31 (7) (2011) 1554–1571.
[26] M.B. Vestergaard, H. Ghanizada, U. Lindberg, et al., Human cerebral perfusion, oxygen consumption, and lactate production in response to hypoxic exposure[J], Cerebr. Cortex 32 (6) (2022) 1295–1306.
[27] Z. Shen, L. Jiang, Y. Yuan, et al., Inhibition of G protein-coupled receptor 81 (GPR81) protects against ischemic brain injury[J], CNS Neurosci. Ther. 21 (3) (2015) 271–279.
[28] E. De Smaele, F. Zazzeroni, S. Papa, et al., Induction of gadd45beta by NF-kappaB downregulates pro-apoptotic JNK signalling[J], Nature 414 (6861) (2001) 308–313.
[29] Q. Chen, Y.Q. Lei, J.F. Liu, et al., Triptolide improves neurobehavioral functions, inflammation, and oxidative stress in rats under deep hypothermic circulatory arrest[J], Aging (Albany NY) 13 (2) (2021) 3031–3044.
[30] E. Trakas, Y. Domnina, A. Panigrahy, et al., Serum neuronal biomarkers in neonates with congenital heart disease undergoing cardiac surgery[J], Pediatr. Neurol. 72 (2017) 56–61.
[31] Y. Sui, L. Stehno-Bittel, S. Li, et al., CXCL10-induced cell death in neurons: role of calcium dysregulation[J], Eur. J. Neurosci. 23 (4) (2006) 957–964.

[32] D.J. Mahad, S.J. Howell, M.N. Woodroofe, Expression of chemokines in the CSF and correlation with clinical disease activity in patients with multiple sclerosis [J], J. Neurol. Neurosurg. Psychiatry 72 (4) (2002) 498–502.
[33] K. Chen, Y. Sun, Y. Diao, et al., alpha7 nicotinic acetylcholine receptor agonist inhibits the damage of rat hippocampal neurons by TLR4/Myd88/NFkappaB signaling pathway during cardiopulmonary bypass[J], Mol. Med. Rep. 16 (4) (2017) 4770–4776.
[34] Z. Nan, Z. Jin, C. Huijuan, et al., Effects of TLR3 and TLR9 signaling pathway on brain protection in rats undergoing sevoflurane pretreatment during cardiopulmonary bypass, Biomed Res Int 2017 (2017), 4286738.
[35] L.N. Tu, A.E. Timms, N. Kibiryeva, et al., Transcriptome profiling reveals activation of inflammation and apoptosis in the neonatal striatum after deep hypothermic circulatory arrest[J], J. Thorac. Cardiovasc. Surg. 158 (3) (2019) 882–890 e4.
[36] M. Ruat, E. Traiffort, Roles of the calcium sensing receptor in the central nervous system[J], Best Pract. Res. Clin. Endocrinol. Metabol. 27 (3) (2013) 429–442.
[37] E. Kallay, Editorial: physiology and pathophysiology of the extracellular calcium-sensing receptor[J], Front. Physiol. 9 (2018) 413.
[38] G. Comito, L. Ippolito, P. Chiarugi, et al., Nutritional exchanges within tumor microenvironment: impact for cancer aggressiveness[J], Front. Oncol. 10 (2020) 396.
[39] D. Hamel, M. Sanchez, F. Duhamel, et al., G-protein-coupled receptor 91 and succinate are key contributors in neonatal postcerebral hypoxia-ischemia recovery [J], Arterioscler. Thromb. Vasc. Biol. 34 (2) (2014) 285–293.
[40] L. Peruzzotti-Jametti, J.D. Bernstock, N. Vicario, et al., Macrophage-derived extracellular succinate licenses neural stem cells to suppress chronic neuroinflammation[J], Cell Stem Cell 22 (3) (2018) 355–368 e13.
[41] P.K. Langston, M. Shibata, T. Horng, Metabolism supports macrophage activation[J], Front. Immunol. 8 (2017) 61.
[42] K.J. Harber, K.E. De Goede, S.G.S. Verberk, et al., Succinate is an inflammation-induced immunoregulatory metabolite in macrophages[J], Metabolites 10 (9) (2020).
[43] D. Ortiz-Masia, L. Gisbert-Ferrandiz, C. Bauset, et al., Succinate activates EMT in intestinal epithelial cells through SUCNR1: a novel protagonist in fistula development[J], Cells 9 (5) (2020).
[44] J. Zhang, Q. Zhang, Y. Yang, et al., Association between succinate receptor SUCNR1 expression and immune infiltrates in ovarian cancer[J], Front. Mol. Biosci. 7 (2020) 150.
[45] E.M. Palsson-Mcdermott, L. a J. O'neill, Targeting immunometabolism as an anti-inflammatory strategy[J], Cell Res. 30 (4) (2020) 300–314.
[46] A.G. Schwaid, K.B. Spencer, Strategies for targeting the NLRP3 inflammasome in the clinical and preclinical space[J], J. Med. Chem. 64 (1) (2021) 101–122.
[47] A.C. Ariza, P.M. Deen, J.H. Robben, The succinate receptor as a novel therapeutic target for oxidative and metabolic stress-related conditions[J], Front. Endocrinol. 3 (2012) 22.
[48] J. Connors, N. Dawe, J. Van Limbergen, The role of succinate in the regulation of intestinal inflammation[J], Nutrients 11 (1) (2018).
[49] J. Xu, Y. Zheng, Y. Zhao, et al., Succinate/IL-1beta signaling Axis promotes the inflammatory progression of endothelial and exacerbates atherosclerosis[J], Front. Immunol. 13 (2022), 817572.
[50] Y. Guo, C. Xie, X. Li, et al., Succinate and its G-protein-coupled receptor stimulates osteoclastogenesis[J], Nat. Commun. 8 (2017), 15621.